Effects of slow highly charged ion irradiation on metal oxide semiconductor capacitors

Daniel B. Cutshall, Dhruva D. Kulkarni, James E. Harriss, Daniel A. Field, Chad E. Sosolik, and William R. Harrell

Citation: Journal of Vacuum Science & Technology B **36**, 052901 (2018); doi: 10.1116/1.5028149
View online: https://doi.org/10.1116/1.5028149
View Table of Contents: http://avs.scitation.org/toc/jvb/36/5
Published by the American Vacuum Society

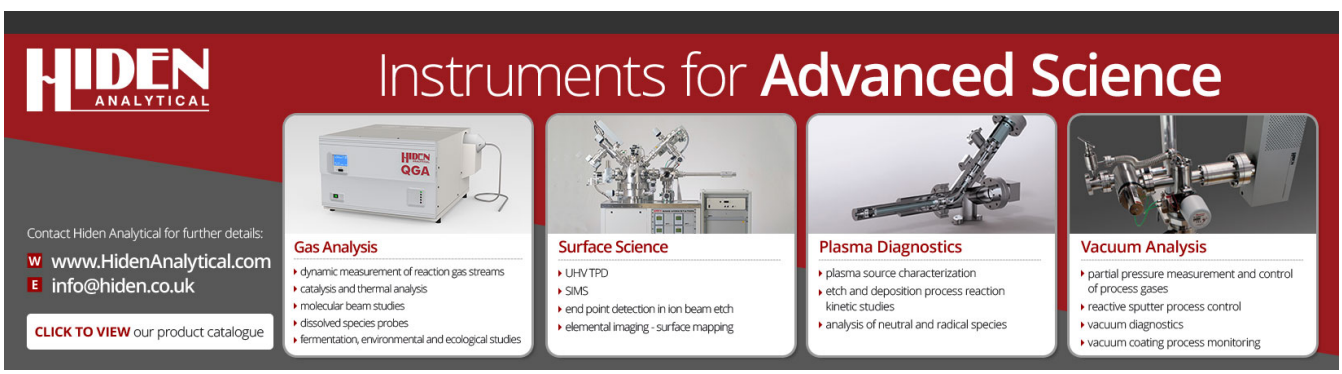

Effects of slow highly charged ion irradiation on metal oxide semiconductor capacitors

Daniel B. Cutshall,[1,a)] Dhruva D. Kulkarni,[2] James E. Harriss,[2] Daniel A. Field,[2] Chad E. Sosolik,[2] and William R. Harrell[1]
[1]*Department of Electrical and Computer Engineering, Clemson University, 433 Calhoun Dr, Clemson, South Carolina 29634*
[2]*Department of Physics and Astronomy, Clemson University, Clemson, South Carolina 29631*

(Received 7 March 2018; accepted 10 July 2018; published 27 July 2018)

Measurements were performed to characterize and better understand the effects of slow highly charged ion (HCI) irradiation, a relatively unexplored form of radiation, on metal oxide semiconductor (MOS) devices. Si samples with 50 nm SiO_2 layers were irradiated with ion beams of Ar^{Q+} (Q = 4, 8, and 11) at normal incidence. The effects of the irradiation were encapsulated with an array of Al contacts forming the MOS structure. High frequency capacitance–voltage (CV) measurements reveal that the HCI irradiation results in stretchout and shifting of the CV curve. These changes in the CV curve are attributed to dangling Si bond defects at the Si/SiO_2 interface and trapped positive charge in the oxide, respectively. Charge state dependencies have been observed for these effects with the CV curve stretchout having a dependence of $Q^{\sim 1.7}$ and the CV curve shifting with a dependence of $Q^{\sim 1.8}$. These dependencies are similar to the results of previous studies focused on the Q-dependence of the stopping power of HCIs. *Published by the AVS.*
https://doi.org/10.1116/1.5028149

I. INTRODUCTION

Over the past couple of decades, there have been several studies devoted to investigating the properties of highly charged ions (HCIs) as well as their potential applications.[1–14] This interest in HCIs stems from their primary distinguishing feature relative to singly charged ions, which is their much larger potential energies due to charge states $Q \gg 1$. The potential energy of an HCI is equal to the sum of the binding energies of the electrons that are removed to create the HCI. This potential energy causes the HCIs to interact in a fundamentally different way with surfaces as compared to singly charged ions, particularly in the case when the kinetic energy is relatively low ($\leq$keV range). An HCI will begin to extract charge from the surface to neutralize while it is still a few nanometers away from the surface. This process is known as over-the-barrier neutralization and was first observed and described in the early 1990s.[15,16] It is important to note that over-the-barrier capture of electrons for neutralization outside the target does not lead directly to a ground-state neutral configuration for the impacting HCI. Instead, what is formed is an unstable partially neutralized ion with electrons in high lying (Rydberg) orbitals. These electrons have been observed to undergo a multitude of processes as the ion reaches the surface. For example, the electrons can be knocked off upon impact with the surface, the electrons can fall into lower atomic levels and emit electromagnetic radiation to conserve energy, or the electrons can, in the presence of other electrons on the ion, be involved in multielectron deexcitation processes (Auger deexcitation). Because slow HCIs deposit their potential energies at and right beneath the surface of target materials within a nanometer-sized region, there is a high density of energy deposition compared to singly charged ion interactions. Several groups have investigated interactions of HCIs with various substrates ranging from insulating dielectrics to conducting metals. In most cases, the effects of a single HCI can be observed on the surface as either a hillock or a crater with dimensions on the order of nanometers.[1] There have also been several groups investigating the possibility of using HCIs for various aspects of nanofabrication including surface cleaning and deposition.[2–14]

Two other application areas in which HCIs are relevant are fusion reactors[17] and outer space operations.[18,19] Whether we are considering space exploration or maintaining appropriate conditions inside a nuclear reactor, having sensors to monitor the environment is critical. Metal oxide semiconductor (MOS) devices could serve as a good candidate for sensing in these areas for a couple of reasons. First, MOS devices permeate nearly all aspects of modern electronics, making them easy to integrate with most existing systems. Second, MOS technology is intrinsically sensitive to radiation since charge imbalances caused by the introduction of trapped charge in the oxide, interface traps, and bulk oxide traps lead to changes in device characteristics.[20] This sensitivity is an obvious advantage when designing radiation sensing technology.

As a basis for designing MOS sensors to monitor this unique type of radiation, it is important to develop an understanding of exactly how these devices respond to exposure to slow HCIs since very little work has been published on this topic. This is especially important, as the general natures of HCI–solid and HCI–surface interactions are not as well explored as those involving singly charged ions. This can be traced primarily to the relatively short time frame that HCIs have been accessible in laboratory environments at reasonable costs.[21] In this work, we investigate the effects of HCIs

[a)]Electronic mail: dcutsha@g.clemson.edu

with 1 keV of kinetic energy on MOS capacitors. Our overall goal is to provide a foundation for future work that will create devices that are capable of accurately monitoring HCIs in outer space, in fusion reactors, and for other potential applications.

II. EXPERIMENT

In this work, we have exposed oxidized silicon samples to a beam of HCIs. After the HCI irradiation, metal contacts were deposited in order to complete the metal oxide semiconductor structure and encapsulate the HCI irradiated oxides, thus allowing us to track the changes caused by the HCI irradiation.[22]

A. Device fabrication

Oxidized silicon wafers were purchased from Si-Tech with an SiO_2 top layer of 50 nm ± 5%. The silicon substrate was p type ($\rho = 5$–$10\ \Omega$ cm) with ⟨100⟩ orientation. SiO_2 was removed from the back of the wafers by a backside etch procedure in which the bare 100 mm wafers were placed face down on supports and a few drops of 49% hydrofluoric acid were placed on the back of the wafers. After the acid had removed the oxide, revealing a hydrophobic Si surface, the wafers were flipped vertical and flushed with flowing deionized (DI) water to prevent the acid from reaching the wafers' front sides. The wafers were then rinsed in three successive DI water baths. After being blown dry with nitrogen, the wafers were immediately placed in a thermal evaporator where backside aluminum ohmic contacts of ∼1 μm thickness were deposited. Following evaporation, the wafers were sintered in a quartz furnace at 450 °C with a nitrogen purge for 35 min. The wafers were cooled to room temperature, and then the silicon wafers were cleaved into square samples of approximately 12 mm × 12 mm. The samples were stored in rough vacuum until irradiation. After irradiation, an array of aluminum contacts was deposited on top of the SiO_2 via thermal evaporation through a shadow mask. The circular topside contacts were approximately 0.5 μm thick and 1 mm in diameter with a center-to-center spacing of 2.5 mm. Ideally, the fabrication of the topside contacts results in a 5 × 5 array of MOS capacitors as shown in Fig. 1; however, due to slight misalignments during thermal evaporation some samples had fewer than 25 capacitors. In this experiment, there were nine samples that were irradiated with HCI beams of various charge states and fluences as described below, and one pristine sample that served as the control.

B. HCI irradiation

The highly charged ion irradiation was performed with the Clemson University Electron Beam Ion Trap (CUEBIT). The CUEBIT setup and basic operation have been reported in detail elsewhere,[23] and some previous results with electronic devices irradiated with the CUEBIT have also been reported.[24,25] The 12 mm × 12 mm Si/SiO_2 samples were mounted on a stainless steel platen and loaded into the CUEBIT target chamber. The base pressure of the target

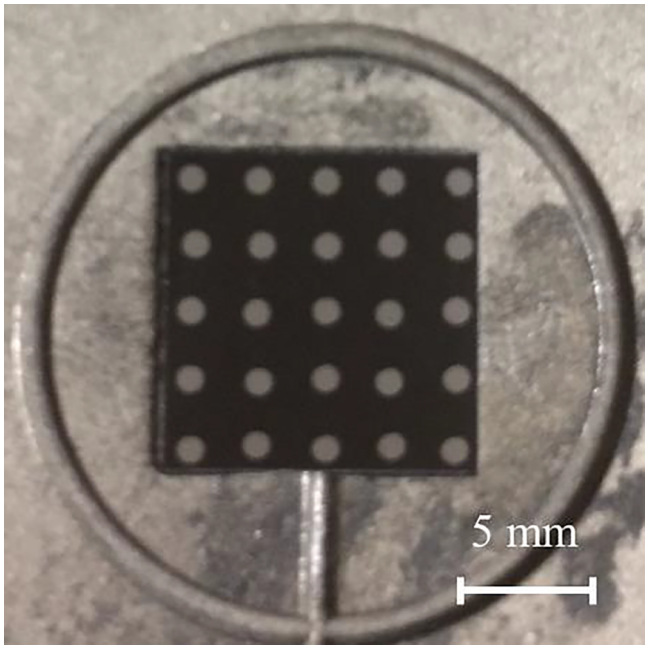

FIG. 1. Si/SiO_2 sample containing 25 MOS capacitors arranged in a 5 × 5 array.

chamber was $\sim 1 \times 10^{-8}$ Torr, and the pressure in the beamline was in the low 10^{-9} Torr range. No external bias was applied to the samples while they were being irradiated, but the backsides of the samples were grounded. In total, there were nine samples irradiated with Ar^{Q+} beams at normal incidence. Specifically, three samples were irradiated for each of the following charge states: Q = 4, 8, and 11, which have potential energies of 138, 567, and 2004 eV, respectively. Beams of the desired charge state were directed onto the sample by means of an analyzing magnet between the source and the target chamber. The kinetic energy of all the ion beams incident on the samples was approximately 1 keV.[26] This was achieved with a custom deceleration lens in front of the target chamber. Beam currents were measured at various times throughout each irradiation using a Faraday cup in the same plane as that of the sample. Based on the measured beam currents, the nominal ion fluences were calculated to be in the range of $\sim 3 \times 10^{13}$ to $\sim 1 \times 10^{14}$ ions/cm^2. All Ar^{Q+} beams produced by the EBIT were observed to be Gaussian in nature as determined by a beam viewer (HRBIS-4000 from Beam Imaging Solutions) and Faraday cup measurements. A typical Ar beam profile is shown in Fig. 2 for the case Q = 8. The FWHM of the HCI beams was ∼3 mm.

C. Device characterization

In order to characterize the effects of the HCI irradiations on our devices, high frequency capacitance–voltage (HFCV) curves were measured for each capacitor (up to 25 per sample) using an HP 4280A 1 MHz CV meter. All CV measurements were performed in a probe station which shielded the sample from light, vibration, and electromagnetic interference. The sample was held in place with a vacuum chuck,

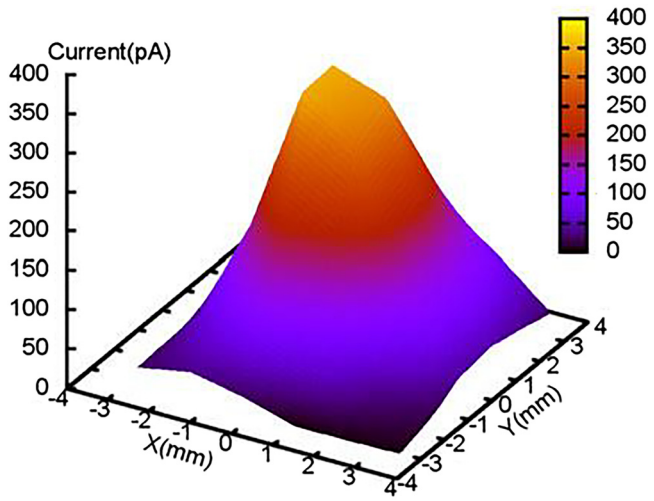

FIG. 2. Typical beam profile for Ar^{Q+} irradiation (Q = 8 is shown).

and micromanipulator controlled probe tips were used to make electrical contact to the device. Only postirradiation measurements were possible due to the topside contacts being deposited after the irradiation. HFCV measurements were also performed on several pristine capacitors that never entered the target chamber and which served as a control or proxy for preirradiation measurements. The CV data for the pristine devices showed good uniformity across the sample, indicating that any changes observed in other samples arise purely from effects of the HCI irradiation.

III. RESULTS AND DISCUSSION

A. Radiation effects on CV characteristics of MOS capacitors

In order to analyze the effects of the HCI irradiation on the MOS capacitors, we extracted information related to three parameters for each CV curve: the flatband voltage (V_{FB}), the midgap voltage (V_{MG}), and the inversion voltage (V_{INV}). The midgap voltage corresponds to the point where the silicon surface is intrinsic, and the inversion voltage corresponds to the onset of strong inversion at the silicon surface. These key indicators were obtained by calculating the flatband, midgap, and inversion capacitances (C_{FB}, C_{MG}, and C_{INV}, respectively) using the methods described in Sze and Ng,[27] Schroder,[28] and Colinge and Colinge[29] and then using the measured CV data to determine the corresponding voltages. These voltages can track two important changes in the CV curve: shifts and stretchout. Shifts refer to translational movement of the entire CV curve along the applied voltage axis, and stretchout refers to changes in the difference between any two of the voltages. The significance of these voltages can be better understood with the help of Fig. 3, which illustrates the band diagrams of the MOS system under various bias conditions. As the bias on the topside contact is made increasingly more positive relative to the semiconductor, the bands of the semiconductor bend down from the flatband by an increasing amount. For the band bending between the flatband condition, Fig. 3(a), and the onset of strong inversion, Fig. 3(c), it can be seen that the semiconductor Fermi level (E_F) at the Si/SiO_2 interface is effectively moving through a significant portion of the semiconductor bandgap. This movement of the Fermi level can be used to qualitatively investigate interface traps and their density as a function of energy, $D_{it}(E)$, in the Si bandgap.

Now we will consider what can be determined from analyzing these three key voltages for the CV curves shown in Fig. 4, which were measured on two of our samples.[25] The red solid curve is from a capacitor on the pristine sample and serves as a control. The blue dashed curve is from a capacitor on a sample that was irradiated with Ar^{8+} and serves as a good representative for devices that experienced significant irradiation (i.e., devices that were spatially aligned with the peak of the beam's Gaussian distribution). Upon initial inspection, the only difference between the two curves in Fig. 4 appears to be that the curve for the irradiated device has experienced a large shift toward more negative voltages. Making the reasonable assumption that defect centers at the Si/SiO_2 interface are acceptor type above the middle of the bandgap and donor type below the middle of the bandgap, it can be inferred that changes in the midgap voltage do not

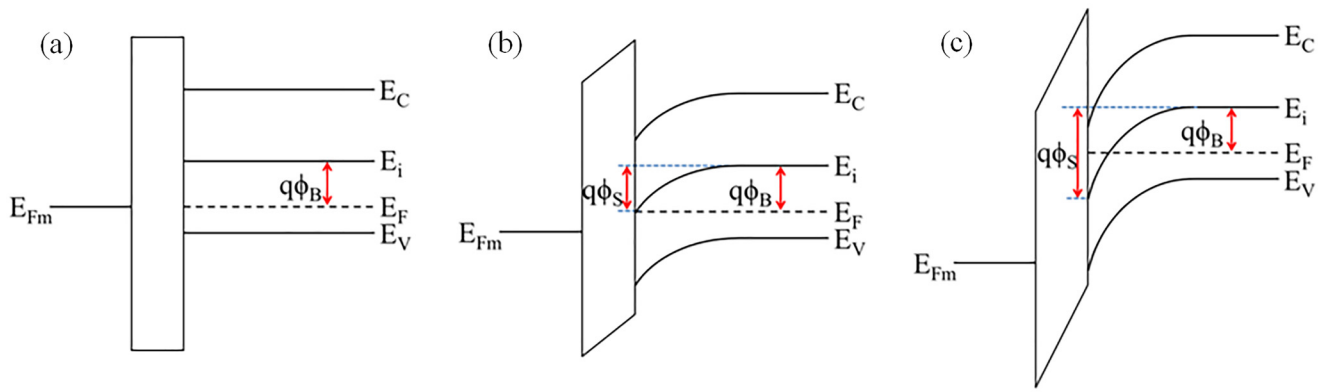

FIG. 3. Band diagram of the MOS system illustrating the three modes of interest focused on here: (a) flatband, (b) midgap where the semiconductor is intrinsic at the Si/SiO_2 interface ($q\phi_S = q\phi_B$), and (c) the onset of strong inversion ($q\phi_S = 2q\phi_B$). $q\phi_S$ is the total band bending and $q\phi_B$ is the Fermi level in the semiconductor bulk.

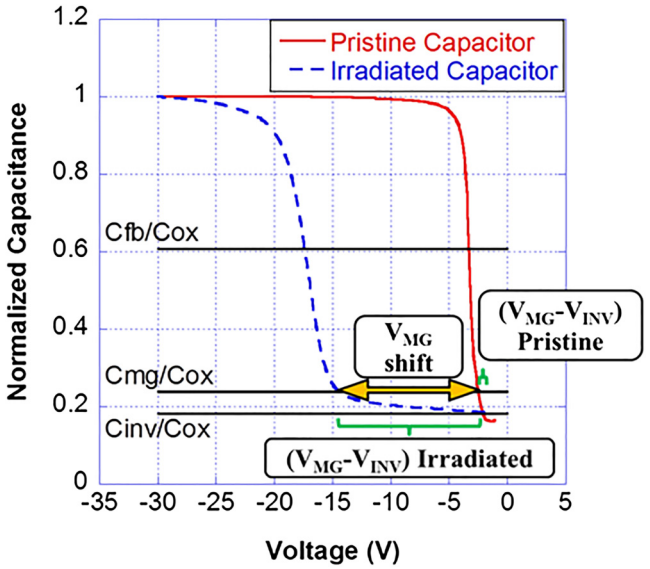

FIG. 4. CV curves for two different capacitors on separate samples. One sample was irradiated and the other one is pristine. Sample was irradiated with Ar^{8+} to a fluence of 4.20×10^{13} ion/cm^2. The midgap shift and stretchout between midgap and inversion points are also shown.

originate from defect centers at the interface. With no influence from interface traps at the midgap point, the increase of $|V_{MG}|$ in our data indicates the presence of some type of positive charge trapped in the oxide.[27] Upon closer inspection of the curves in Fig. 4, it is evident that the V_{INV} is approximately the same for both the pristine device and the irradiated device. This indicates that a significant amount of stretchout between midgap and inversion is occurring for the irradiated devices in addition to the translational shift. The combination of stretchout and shift was observed for the capacitors that were significantly affected by the HCI irradiation, but it should be noted that some of the capacitors toward the edge of the sample behaved similar to the pristine devices due to the sample size being larger than the FWHM of the HCI beam.

The stretchout in the CV curves indicates the presence of interface traps at the Si/SiO_2 interface of the irradiated capacitors.[27,28] The small rate of increase for the measured capacitance between the inversion and midgap points indicates that the interface traps are somewhat localized around one energy in the silicon bandgap, and therefore are likely predominantly due to one type of defect. This can be understood by considering the extreme case of infinite D_{it} at a specific energy level in the Si bandgap. As more charge is applied to the metal contact of the MOS device, the interface traps will adjust their occupancy in order to balance the charge applied on the metal. Because there are an infinite number of interface traps at that energy level, the effective position of the Fermi level at the interface does not need to change in order to balance the charge on the metal. No change in the Fermi level position at the interface means no change in the depletion width in the Si, and consequently no change in the capacitance. For the case of a large (but finite) D_{it}, the effective Fermi level position at the interface will change more slowly with changes in bias past the energy level where interface traps are most dense. The slow change in position of the Fermi level at the interface in the bandgap corresponds to a small rate of change for the depletion width as well as the overall capacitance. As illustrated in Figs. 3(b) and 3(c), the Fermi level at the interface is in the upper half of the band gap for voltages between V_{MG} and V_{INV}. Since almost all of the stretchout in the CV curves occurs between the inversion and midgap points, we know that the largest density of interface traps is in the upper half of the band gap. Knowing that the bulk potential of the Si substrate is approximately $q\phi_B = 0.31$ eV (based on the average resistivity), we can more precisely say that the distribution of interface states exists somewhere between the middle of the band gap, E_i, and an energy level of 0.31 eV above E_i.

It is likely that defects at the interface of the irradiated devices were created by a two-stage process involving the interaction of holes with defect centers in the oxide, hydrogen, and P_b centers at the interface as described in the literature.[30–36] Holes in the oxide can be created by the HCIs in a couple of different ways. As an HCI approaches, but before it actually impacts the sample, it begins capturing electrons from the surface. As electrons are removed from the surface, an abundance of holes will begin accumulating in the SiO_2 below the HCI in the nanometer-scale region. When the HCI impacts the sample, several electron–hole pairs will be created as with singly charged ion irradiation.[1,11,37,38] Due to the large disparity of mobilities for electrons and holes in SiO_2, 20 cm^2/V s and 4×10^{-9} cm^2/V s, respectively,[39] there will be a large portion of electrons that move away from the HCI impact site before recombination can occur. Since there is no applied bias during irradiation, the dispersion of holes throughout the oxide will result primarily from diffusion. Simulations using the stopping and range of ions in matter program indicate that the neutralized argon atoms will come to rest only a few nanometers into the SiO_2 layer and will have a negligible effect on the behavior of the MOS devices. It is the created holes and their subsequent diffusion toward the interface that result in device damage in the bulk and at the interface. The first stage of the two-stage process for interface trap creation involves the capture of a hole at a defect site in the oxide. The dominant oxide hole trap in SiO_2 is due to an oxygen vacancy, which becomes a positively charged E′ center after capturing a hole.[30,36] The E′ centers which are near the interface are then able to interact with H-passivated Si dangling bonds at the Si/SiO_2 interface. This is the second stage of the process. Lenahan and Conley have claimed that hydrogen will be exchanged between E′ centers in the oxide and Si dangling bonds at the interface via the following equation:[31]

$$\lambda H_2 + P_b H + E' \leftrightarrow \lambda H_2 + P_b + E'H, \quad (1)$$

where λ indicates the relative abundance of diatomic hydrogen and is used to balance the equation. As hydrogen is exchanged between the oxide traps and the interface traps, there is no net change in charge for either defect site. The

end results of this process are positively charged defects in the oxide, which are responsible for the shift seen in V_{MG}, and Si dangling bond defects at the Si/SiO_2 interface, which are responsible for the stretchout. The energy range where our D_{it} is concentrated agrees well with the energy level for the P_{b0} silicon dangling bond defect in ⟨100⟩ silicon as reported by Lenahan.[40] It should be mentioned that several groups have also argued that H^+ ions created from hole trapping in the oxide will react with defect sites at the interface, resulting in molecular hydrogen and a dangling Si bond.[33–35]

B. Data analysis

After each irradiation, we extracted the key parameters (V_{FB}, V_{MG}, V_{INV}, and their differences) for each capacitor on a sample. For example, Fig. 5 shows $|V_{MG} - V_{INV}|$ values for a 5×5 array of capacitors that was irradiated with Ar^{8+}. In order to more accurately discern trends in the data, we have used a Gaussian analysis technique that allowed us to create a reliable average value of the parameter of interest for each sample. Thus, the data for 25 capacitors on one sample are reduced to a single average number. The analysis is performed by creating a 2D Gaussian fit for the voltage data in MATLAB and then calculating an average value for the sample using the following model equation:

$$|V_{MG} - V_{INV}|_{Average} = \frac{\iint_A (\text{Gaussian Fit}) dA}{\iint_A dA}, \quad (2)$$

where the integrations are performed across the area of the sample, A. A two dimensional Gaussian fit of the numerical data shown in Fig. 5 is also overlaid in the figure, illustrating the clear spatial dependence related to the incident beam profile. A similar averaging was performed on the V_{MG} data in order to investigate the charge state dependence of the oxide trapped charge. This analysis technique includes a correction factor which provides a more accurate ion fluence seen by each sample. The correction factor accounts for two potential sources of error. The first is the difference in size between the Faraday cup used to measure the beam current and the sample being irradiated. The second potential source of error that is corrected for is any slight misalignment between the sample and the beam that might have occurred during irradiation. We note that this data analysis technique using 2D Gaussian fits and a correction factor has been employed to investigate V_{FB} shifts in our previous work.[24]

C. Charge state dependence

Figure 6 shows the results of the analysis of the midgap to inversion stretchout data for all nine samples that were irradiated. The average difference between midgap and inversion points for the pristine sample was 0.21 V. The results in Fig. 6 indicate that the fluences used in these experiments were such that the effect on the MOS devices is approaching saturation, and for the case of the Ar^{11+} data, the effect is diminished at the highest fluence. One possible reason for this is a competing annealing process that becomes more dominant as irradiation times increase. This type of effect has been observed in Schottky diodes exposed to swift heavy ions.[41–44] The higher charge state beams produced in the EBIT have lower beam currents; therefore, devices

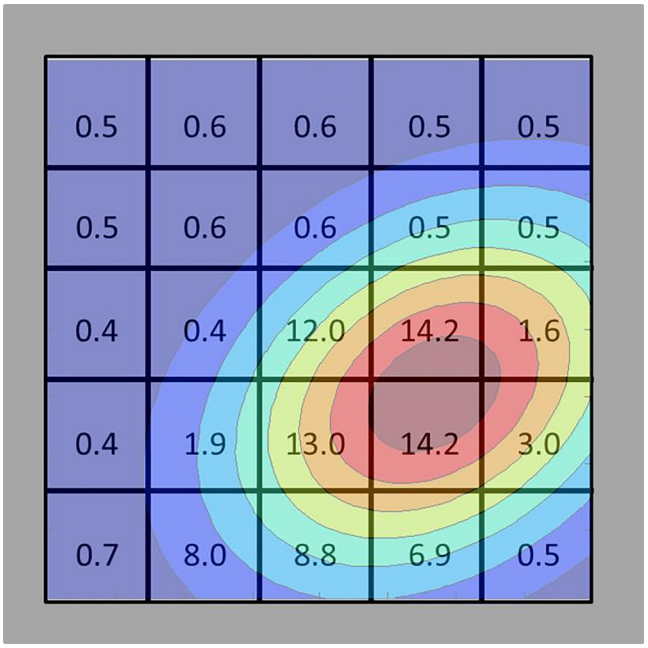

FIG. 5. Numerical representation of the stretchout between midgap and inversion in volts for the 5×5 capacitor array shown in Fig. 1 (i.e., the $|V_{MG} - V_{INV}|$ values for the 25 capacitors) with the 2D Gaussian fit overlaid ($R^2 = 0.9407$). The stretchout values of the Gaussian fit range from approximately 0.5 V to a little above 14 V.

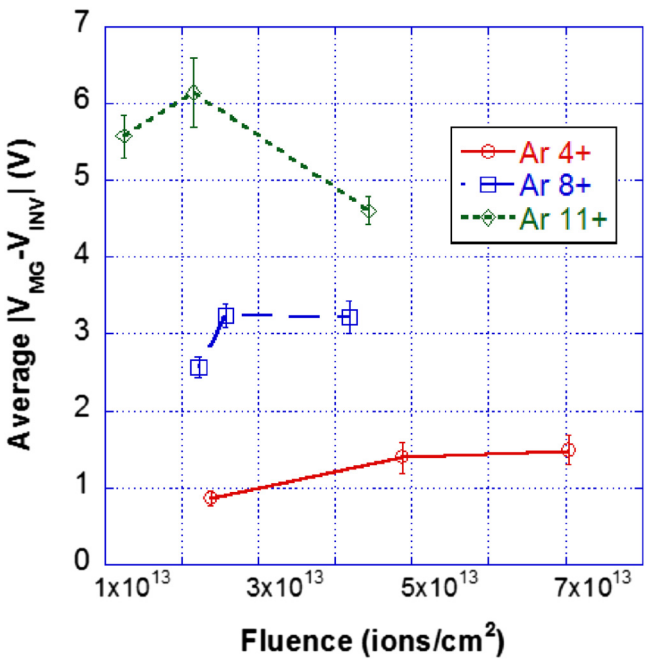

FIG. 6. Average $|V_{MG} - V_{INV}|$ values for each of the nine irradiated samples. Sample averages were obtained by using the 2D Gaussian fit of the voltage data. The correction factor mentioned in Subsec. III B was used to determine the fluences used in this plot.

irradiated at higher charge states require a longer irradiation time to reach a given fluence compared to devices irradiated with lower charge states. So, it is possible that the longer irradiation time for the highest fluence point for the Ar^{11+} data set shows a reduced effect due to an increased amount of room-temperature annealing.

Because our fluences appear to be in the saturation regime, we were unable to gain any useful information by investigating the rate of change in $|V_{MG} - V_{INV}|$ with respect to fluence as we have done previously with V_{FB} data.[24] As an alternative, we have calculated the average effect observed for a given charge state across all fluences. Because we are interested in the change in the stretchout, $\Delta|V_{MG} - V_{INV}|$, the value of $|V_{MG} - V_{INV}|$ recorded for the capacitors on the pristine sample was subtracted from the average $|V_{MG} - V_{INV}|$ for a given charge state. In essence, we are using the pristine sample as a proxy for preirradiation measurements, since top contacts were deposited after irradiation. The result of this calculation is $\Delta|V_{MG} - V_{INV}|$ as a function of charge state as shown in Fig. 7. A power law fit to the data shows that the stretchout between midgap and inversion voltages varies as approximately $Q^{\sim 1.7}$.

The result of applying our analysis technique to the V_{MG} data is shown in Fig. 8 for all nine samples that were irradiated. The average magnitude of the midgap voltage for the pristine sample was 1.24 V. Just as with the $|V_{MG} - V_{INV}|$ data for the Ar^{11+}, it is clear that the effects actually begin to lessen for the highest fluence levels for all charge states. As mentioned earlier, this is possibly due to an annealing effect which becomes more prominent as irradiation times are increased. Because the ion fluences are not in a linear regime, the data points for each charge state were averaged such that each charge state is represented by a single average V_{MG} value. The average value of V_{MG} for the pristine capacitors was then subtracted from these averages in order to track the ΔV_{MG} as a function of charge state. The results of this analysis are shown in Fig. 9. Applying a power law fit to these data indicates that the shift in V_{MG} varies as approximately $Q^{\sim 1.8}$.

These results indicate that the creation of both oxide and interface traps has approximately the same Q dependency. This Q dependency is also similar to the power law that we observed for V_{FB} shifts in thicker oxides after HCI irradiation[24] ($\sim Q^{2.2}$). It is also important to note that the energy loss of HCIs in thin carbon membranes has been reported to display quadratic dependence on the charge state.[45] The commonality between the Q-dependent changes in our CV curves and the Q-dependent energy loss should not be dismissed as coincidence, but rather this similarity could be interpreted as indicating that there is some intrinsic relationship between the internal mechanisms of energy loss for HCIs in solids and the resultant damage that we observe in our electrical characterization measurements. Numerical modeling, similar to what has been performed for ionizing radiation incident on MOS capacitors,[46] could provide additional insight into the charge state dependent effects produced in electronic devices and materials; however, care would need to be taken to account for the unique properties of slow HCIs (i.e., low kinetic energy and relatively high potential energy). Future experimental work will focus on varying the fluence, kinetic energy, and incidence angle of different ion species. Hopefully, the results will provide a deeper understanding of HCI effects on electronic materials and devices.

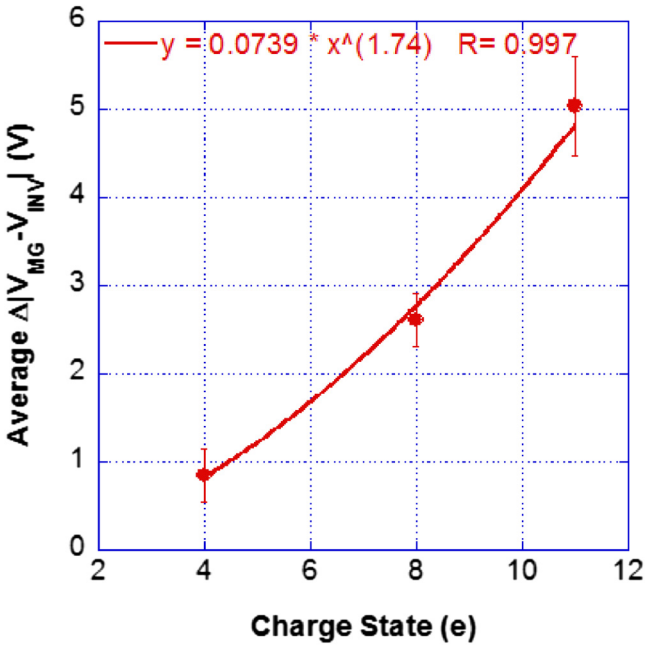

FIG. 7. Average stretchout between midgap and inversion for all samples of a given charge state minus the corresponding stretchout seen in the pristine sample. Also shown is a power law fit showing that stretchout between midgap and inversion varies as $Q^{\sim 1.7}$.

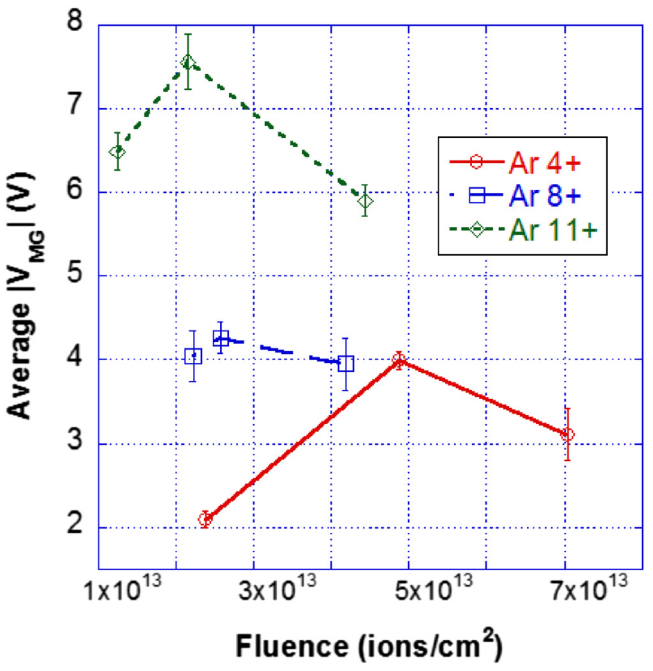

FIG. 8. Average V_{MG} values for each of the nine irradiated samples. Sample averages were obtained by using the 2D Gaussian fit of the voltage data. The correction factor mentioned in Subsec. III B was used to determine the fluences used in this plot.

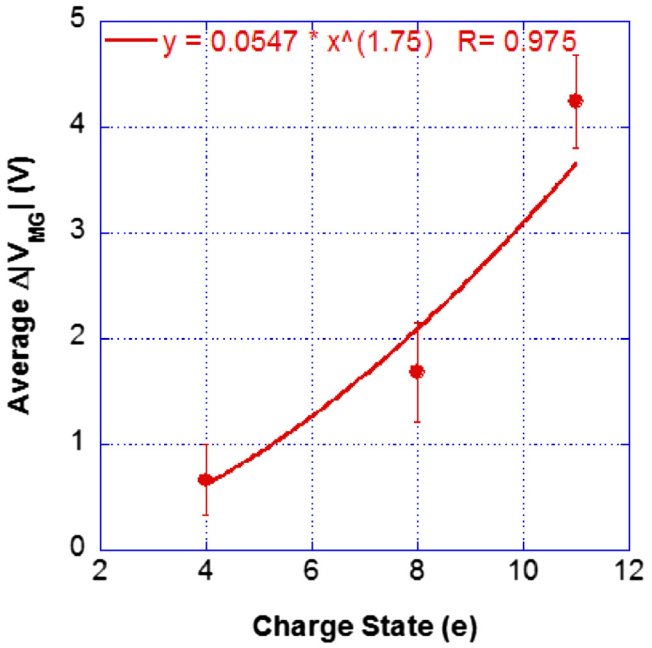

FIG. 9. Average midgap voltage for all samples of a given charge state minus the average midgap voltage seen in the pristine sample. Also shown is a power law fit showing that shifts of the midgap voltage vary as $Q^{\sim 1.8}$.

IV. CONCLUSION

We have irradiated Si/SiO_2 samples with slow HCIs in an electron beam ion trap facility at Clemson University in order to gain a better understanding of how this relatively unexplored type of radiation affects electronic devices. The samples consisted of an array of top metal contacts evaporated postradiation to form MOS capacitors, and HFCV curves showed a translation of V_{MG} and an increase in the stretchout between inversion and midgap compared to pristine capacitors. These changes indicate the creation of oxide trapped charges and interface traps, respectively. It was determined that the oxide trapped charges were most likely due to E' centers, and the interface traps were most likely due to P_b defects. Using a data analysis technique based on a 2D Gaussian fit of the voltage data, we found a charge state dependence of $Q^{\sim 1.7}$ for the stretchout of the CV curves between midgap and inversion, and a charge state dependence of $Q^{\sim 1.8}$ for the shift in V_{MG}. This work provides a good foundation for future applications related to fusion reactors and outer space operations by providing a better understanding of how MOS devices are affected by HCI irradiation. Current research is being pursued using Schottky diodes as sensors, and future work is planned for MOS irradiations with thin metal contacts (~20 nm) deposited prior to HCI irradiation.

[1]F. Aumayr, S. Facsko, A. S. El-Said, C. Trautmann, and M. Schleberger, J. Phys. Condens. Matter **23**, 393001 (2011).
[2]T. Schenkel, M. Schneider, M. Hattass, M. W. Newman, A. V. Barnes, A. V. Hamza, D. H. Schneider, R. L. Cicero, and C. E. D. Chidsey, J. Vac. Sci. Technol. B **16**, 3298 (1998).
[3]K. Kuroki, N. Okabayashi, H. Torii, K. Komaki, and Y. Yamazaki, Appl. Phys. Lett. **81**, 3561 (2002).
[4]M. Tona, S. Takahashi, K. Nagata, N. Yoshiyasu, C. Yamada, N. Nakamura, and S. Ohtani, Appl. Phys. Lett. **87**, 224102 (2005).
[5]N. Okabayashi, K. Komaki, and Y. Yamazaki, Nucl. Instrum. Methods Phys. Res. B **232**, 244 (2005).
[6]M. Tona, K. Nagata, S. Takahashi, N. Nakamura, N. Yoshiyasu, M. Sakurai, C. Yamada, and S. Ohtani, Nucl. Instrum Methods Phys. Res. B **232**, 249 (2005).
[7]S. Takahashi, M. Tona, K. Nagata, N. Nakamura, N. Yoshiyasu, C. Yamada, S. Ohtani, and M. Sakurai, Appl. Phys. Lett. **87**, 063111 (2005).
[8]M. Tona, K. Nagata, S. Takahashi, N. Nakamura, N. Yoshiyasu, M. Sakurai, C. Yamada, and S. Ohtani, Surf. Sci. **600**, 124 (2006).
[9]M. Tona, H. Watanabe, S. Takahashi, N. Nakamura, N. Yoshiyasu, M. Sakurai, C. Yamada, and S. Ohtani, Nucl. Instrum. Methods Phys. Res. B **258**, 163 (2007).
[10]M. Sporn *et al.*, Phys. Rev. Lett. **79**, 945 (1997).
[11]I. P. Jain and G. Agarwal, Surf. Sci. Rep. **66**, 77 (2011).
[12]G. Borsoni *et al.*, Solid State Electron. **46**, 1855 (2002).
[13]M. Tona *et al.*, Nucl. Instrum. Methods Phys. Res. B **256**, 543 (2007).
[14]M. Sakurai *et al.*, Nucl. Instrum. Methods Phys. Res. B **257**, 297 (2007).
[15]J. Burgdörfer, P. Lerner, and F. W. Meyer, Phys. Rev. A **44**, 5674 (1991).
[16]R. E. Lake, C. E. Sosolik, and J. M. Pomeroy, Phys. Rev. A **87**, 062901 (2013).
[17]G. Federici *et al.*, Nucl. Fusion **41**, 1967 (2001).
[18]J. R. Schwank, M. R. Shaneyfelt, and P. E. Dodd, IEEE Trans. Nucl. Sci. **60**, 2074 (2013).
[19]F. W. Meyer, P. R. Harris, C. N. Taylor, H. M. Meyer III, A. F. Barghouty, and J. H. Adams, Nucl. Instrum. Methods Phys. Res. B **269**, 1316 (2011).
[20]T. P. Ma and P. V. Dressendorfer, *Ionizing Radiation Effects in MOS Devices and Circuits* (Wiley, Chichester, 1989).
[21]J. W. McDonald and D. H. G. Schneider, Nucl. Instrum. Methods Phys. Res. B **241**, 870 (2005).
[22]R. Shyam, D. D. Kulkarni, D. A. Field, E. S. Srinadhu, J. E. Harriss, W. R. Harrell, and C. E. Sosolik, IEEE Trans. Nucl. Sci. **62**, 3346 (2015).
[23]R. Shyam, D. D. Kulkarni, D. A. Field, E. S. Srinadhu, D. B. Cutshall, W. R. Harrell, J. E. Harriss, and C. E. Sosolik, AIP Conf. Proc. **1640**, 129 (2015).
[24]D. D. Kulkarni, R. E. Shyam, D. B. Cutshall, D. A. Field, J. E. Harriss, W. R. Harrell, and C. E. Sosolik, J. Mater. Res. **30**, 1413 (2015).
[25]D. B. Cutshall, D. D. Kulkarni, A. J. Miller, J. E. Harriss, W. R. Harrell, and C. E. Sosolik, Nucl. Instrum. Methods Phys. Res. B **422**, 47 (2018).
[26]D. D. Kulkarni, C. D. Ahl, A. M. Shore, A. J. Miller, J. E. Harriss, C. E. Sosolik, and J. P. Marler, Rev. Sci. Instrum. **88**, 083306 (2017).
[27]S. M. Sze, and K. K. Ng, *Physics of Semiconductor Devices*, 3rd ed. (Wiley, Hoboken, 2007), pp. 197–236.
[28]D. K. Schroder, *Semiconductor Material and Device Characterization*, 2nd ed. (Wiley, New York, 1998), pp. 337–408.
[29]J. P. Colinge and C. A. Colinge, *Physics of Semiconductor Devices* (Kluwer Academic, Norwell, 2002), pp. 165–187.
[30]J. F. Conley, Jr. and P. M. Lenahan, IEEE Trans. Nucl. Sci. **40**, 1335 (1993).
[31]P. M. Lenahan and J. F. Conley, Jr., IEEE Trans. Nucl. Sci. **45**, 2413 (1998).
[32]B. R. Tuttle, D. R. Hughart, R. D. Schrimpf, D. M. Fleetwood, and S. T. Pantelides, IEEE Trans. Nucl. Sci. **57**, 3046 (2010).
[33]F. B. McLean, IEEE Trans. Nucl. Sci. **NS-27**, 1651 (1980).
[34]D. M. Fleetwood, Microelectron. Reliab. **42**, 523 (2002).
[35]S. N. Rashkeev, D. M. Fleetwood, R. D. Schrimpf, and S. T. Pantelides, Phys. Rev. Lett. **87**, 165506 (2001).
[36]W. L. Warren, M. R. Shaneyfelt, D. M. Fleetwood, J. R. Shwank, and P. S. Winokur, IEEE Trans. Nucl. Sci. **41**, 1817 (1994).
[37]J. D. Gillaspy, J. Phys. B At. Mol. Opt. Phys. **34**, R93 (2001).
[38]W. Ensinger, Radiat. Meas. **40**, 712 (2005).
[39]R. C. Hughes, Appl. Phys. Lett. **26**, 436 (1975).
[40]P. M. Lenahan, Microelectron. Eng. **69**, 173 (2003).
[41]R. Singh, S. K. Arora, and D. Kanjilal, Mater. Sci. Semicond. Process. **4**, 425 (2001).
[42]S. Verma, K. C. Praveen, T. Kumar, and D. Kanjilal, IEEE Trans. Device Mater. Rel. **13**, 98 (2013).
[43]S. Kumar, Y. S. Katharria, Y. Batra, and D. Kanjilal, J. Phys. D Appl. Phys. **40**, 6892 (2007).
[44]A. Bobby, N. Shiwakoti, P. M. Sarun, S. Verma, K. Asokan, and B. K. Antony, Curr. Appl. Phys. **15**, 1500 (2015).
[45]R. A. Wilhelm, E. Gruber, R. Ritter, R. Heller, S. Facsko, and F. Aumayr, Phys. Rev. Lett. **112**, 153201 (2014).
[46]R. K. Chauhan and P. Chakrabarti, Microelectron. J. **33**, 197 (2002).